Atmospheric Pressure and Room Temperature Synthesis of Methanol through Plasma-Catalytic Hydrogenation of CO_2

Li Wang,[†] *Yanhui Yi,*[‡] *Hongchen Guo,*[‡] *and Xin Tu**[†]

[†]Department of Electrical Engineering and Electronics, University of Liverpool, Liverpool, L69 3GJ, UK

[‡]State Key Laboratory of Fine Chemicals, School of Chemical Engineering, Dalian University of Technology, Dalian, 116024, China

ABSTRACT: CO_2 hydrogenation to methanol is a promising process for CO_2 conversion and utilization. Despite a well-developed route for CO hydrogenation to methanol, the use of CO_2 as a feedstock for methanol synthesis remains underexplored, and one of its major challenges is high reaction pressure (usually 30-300 atm). In this work, atmospheric pressure and room temperature (~30 ^oC) synthesis of methanol from CO_2 and H_2 has been successfully achieved using a dielectric barrier discharge (DBD) with and without a catalyst. The methanol production was strongly dependent on the plasma reactor setup; the DBD reactor with a special water-electrode design showed the highest reaction performance in terms of the conversion of CO_2 and methanol yield. The combination of the plasma with Cu/γ-Al_2O_3 or Pt/γ-Al_2O_3 catalyst

significantly enhanced the CO_2 conversion and methanol yield compared to the plasma hydrogenation of CO_2 without a catalyst. The maximum methanol yield of 11. 3% and methanol selectivity of 53.7% were achieved over the Cu/γ-Al_2O_3 catalyst with a CO_2 conversion of 21.2% in the plasma process, while no reaction occurred at ambient conditions without using plasma. The possible reaction mechanisms in the plasma CO_2 hydrogenation to CH_3OH with and without a catalyst were proposed by combined means of electrical and optical diagnostics, product analysis, catalyst characterization and plasma kinetic modeling. These results have successfully demonstrated that this unique plasma process offers a promising solution for lowering the kinetic barrier of catalytic CO_2 hydrogenation to methanol instead of using traditional approaches (e.g. high reaction temperature and high-pressure process), and has great potential to deliver a step-change in future CO_2 conversion and utilization.

KEYWORDS: CO_2 conversion; Non-thermal plasmas; Plasma-catalysis; CO_2 hydrogenation; Methanol synthesis; Ambient conditions; Synergistic effect

INTRODUCTION

CO_2 is a major greenhouse gas, contributing to global warming and climate change. The largest source of CO_2 emissions is from the burning of fossil fuels for heat, electricity and transportation. The EU has committed to cutting greenhouse gas emissions to 80% below 1990 levels by 2050.[1] The process of capturing CO_2 is the most efficient abatement technique in terms of tons of CO_2 removed from the atmosphere; however, the following carbon storage has significant shortcomings, including high investment costs, uncertainty of potential long-term storage capacity and increased public resistance.[2] Instead of treating CO_2 as a waste for storage,

the use of captured low value CO_2 as a feedstock for the synthesis of higher value platform chemicals and synthetic fuels has attracted significant interest and is regarded as a key element of a future sustainable low carbon economy in chemical and energy industries. CO_2 is considered a strategic molecule for the progressive introduction of renewable energy sources into the chemical and energy chain and is part of the portfolio of critical technologies for curbing CO_2 emissions. However, the activation and conversion of CO_2 into valued-added fuels and chemicals remains a great challenge as CO_2 is a thermodynamically stable molecule and requires a significant amount of energy for its activation. Great efforts have been devoted to overcoming the thermodynamic barriers for CO_2 activation and conversion. A particularly significant route being developed for CO_2 conversion is CO_2 reduction with H_2 which has a lower thermodynamic limitation compared to direct CO_2 decomposition and dry reforming of methane (DRM).

The direct hydrogenation of CO_2 mainly produces three types of C1 chemicals: CH_4 (R1), CO (R2) and CH_3OH (R3).[3-4] CH_4 is a fuel and a major energy source, while CO is an important chemical feedstock for the synthesis of a range of platform chemicals and synthetic fuels through existing processes such as Fischer-Tropsch process and methanol synthesis. As shown in Scheme 1, CO_2 hydrogenation to CH_3OH is one of the most attractive routes for CO_2 conversion and utilization. CH_3OH is a valuable fuel substitute and additive, and is also a key feedstock for the synthesis of other higher value chemicals. In addition, methanol is considered a promising hydrogen carrier, suitable for storage and transportation.

$CO_2 + 4H_2 \rightarrow CH_4 + 2H_2O$, $\Delta H_{298K} = -252.9$ kJ/mol[4] (R1)

$CO_2 + H_2 \rightarrow CO + H_2O$, $\Delta H_{298K} = 41.2$ kJ/mol[4] (R2)

$CO_2 + 3H_2 \rightarrow CH_3OH + H_2O$, $\Delta H_{298K} = -49.5$ kJ/mol[4] (R3)

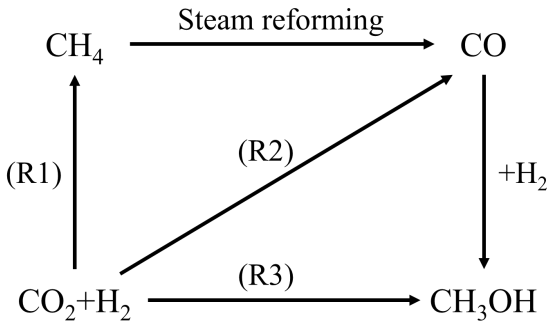

Scheme 1. Direct and indirect approaches for CO_2 hydrogenation to C1 chemicals.

Current research on CO_2 hydrogenation to methanol mainly focusses on the use of heterogeneous catalysis at high pressures.[4-6] Cu-based catalysts have attracted considerable interest for catalytic CO_2 hydrogenation for methanol synthesis,[7-11] owing to the excellent activity of metallic Cu for this reaction.[12-14] Extensive efforts have also been devoted to modifying the structure of Cu-based catalysts using various supports (Al_2O_3, ZnO, ZrO_2, SiO_2, Nb_2O_5, Mo_2C, and carbon materials, etc.), promoters (Zn, Zr, Ce, Ga, Si, V, K, Ti, B, F, and Cr) and preparation methods. [3-5] Behrens et al. compared methanol synthesis from CO_2 hydrogenation and CO hydrogenation over Cu (111), Cu (211) and CuZn (211) facets. They found that CO_2 hydrogenation proceeded via a stepwise formation of adsorbed HCOO, HCOOH, H_2COOH, H_2CO and H_3CO species, while CO hydrogenation formed $HCO_{(ad)}$, $H_2CO_{(ad)}$ and $H_3CO_{(ad)}$ as the key intermediates. [12] To date, most researchers agree that formate (HCOO) and CO are the initial intermediates in CO_2 hydrogenation to methanol on Cu surfaces, and three main reaction pathways have been proposed based on theoretical calculation (Path 1, 2 and 3). Path 1 preferentially occurs on Cu (100) and Cu (111) surfaces, with $HCOO_{(ad)}$ hydrogenation to $H_2COO_{(ad)}$ and $H_2CO_{(ad)}$ through H addition reactions predicted to be the rate limiting steps in Path 1.[15-18] Mavrikakis et al. and Behrens et al. concluded that the hydrogenation of $HCOO_{(ad)}$

was preferable for the formation of $HCOOH_{(ad)}$ instead of $H_2COO_{(ad)}$ on Cu (111), eventually producing methanol via Path 2.[12,19] Unlike Path 1 and 2, Path 3 occurs through the initial hydrogenation of $CO_{2(ad)}$ to $HOCO_{(ad)}$, followed by dissociation of $HOCO_{(ad)}$ to $CO_{(ad)}$ and $OH_{(ad)}$ via the reverse water gas shift (RWGS) reaction. The further hydrogenation of produced $CO_{(ad)}$ can form methanol,[19-21] which has a similar mechanism to that presented for methanol synthesis from syngas.[12]

Path 1: $CO_{2(ad)} \rightarrow HCOO_{(ad)} \rightarrow H_2COO_{(ad)} \rightarrow H_2CO_{(ad)} \rightarrow H_3CO_{(ad)} \rightarrow CH_3OH_{(ad)}$

Path 2: $CO_{2(ad)} \rightarrow HCOO_{(ad)} \rightarrow HCOOH_{(ad)} \rightarrow H_2COOH_{(ad)} \rightarrow H_2CO_{(ad)} \rightarrow H_3CO_{(ad)} \rightarrow CH_3OH_{(ad)}$

Path 3: $CO_{2(ad)} \rightarrow HOCO_{(ad)} \rightarrow CO_{(ad)} \rightarrow HCO_{(ad)} \rightarrow H_2CO_{(ad)} \rightarrow H_3CO_{(ad)} \rightarrow CH_3OH_{(ad)}$

In addition to Cu-based catalysts, Ni-Ga catalysts have been reported to have excellent activity and stability for CO_2 hydrogenation to methanol.[22] Studt et al. found that a Ni_5Ga_3 catalyst exhibited better activity for methanol synthesis in comparison to a conventional $Cu/ZnO/Al_2O_3$ catalyst.[22] They suggested that oxygen adsorption energy (ΔE_O) on metal surfaces is the key factor in methanol synthesis. Weak oxygen binding to metal surfaces results in the formation of unstable intermediates and a high reaction barrier, whilst if the interaction is too strong, surface poisoning occurs due to the formation of strongly adsorbed species. Therefore, a moderate ΔE_O becomes energetically favorable and allows further reaction of intermediates, as well as the desorption of products on the catalyst surfaces. In addition, recent theoretical and experimental studies have shown that oxygen deficient indium oxide (In_2O_3) is a superior catalyst for CO_2 hydrogenation to methanol.[23-25] The creation of different oxygen vacancies on the In_2O_3 (110) surface and their influence on methanol production from CO_2 hydrogenation were investigated through density function theory (DFT) calculation by Ye et al., revealing that CO_2 activation and hydrogenation preferentially takes place on the D4 surface with O_{v4} defective site.[24] Very recently, a In_2O_3/ZrO_2 catalyst was reported to exhibit 100% methanol selectivity and

remarkable stability, (evidenced by a catalyst stability test running the reaction over 1000 h on stream using operating conditions for industrial methanol synthesis), whilst a conventional $Cu/ZnO/Al_2O_3$ catalyst experienced rapid deactivation under the same conditions.[23]

CO_2 hydrogenation to methanol (R3) is favored to occur at low temperatures and high pressures due to the reaction thermodynamics as it is an exothermic and molecule-reducing reaction. However, low-temperature operation suffers from a dynamic limitation in CO_2 activation, in contrast to the thermodynamic limitation of the reaction at high temperatures. In addition, although high temperature facilitates CO_2 activation, the simultaneous formation of CO through the reverse water gas shift is the primary competitive reaction for methanol synthesis in CO_2 hydrogenation. Non-thermal plasma (NTP) technology provides an attractive and promising alternative to thermal catalysis to tackle these challenges facing CO_2 activation. NTP shows a significant superiority in activating thermodynamically stable molecules (e.g., CO_2) over a catalytic process at atmospheric pressure and low temperatures.[26-31] NTP can generate numerous highly energetic electrons with a typical electron energy of 1–10 eV. This has created growing interest in the use of energetic electrons as an alternative 'catalyst' to activate reactants (e.g., CO_2 and H_2) into a range of chemically reactive species (e.g. radicals and excited atoms, ions and molecules) for the initiation and propagation of chemical reactions. Furthermore, the overall gas temperature of NTP can be maintained as low as room temperature.[32]

Interestingly, these unique properties of NTP mean it has great potential to overcome the barriers in catalytic CO_2 hydrogenation to methanol. In addition, plasma processes can be switched on and off instantly to save energy due to fast reaction initiation with high reaction rates and there is great potential for combination with renewable energy sources, especially waste energy from wind or solar power for localized or distributed chemical energy storage. If

the required energy for this process can be supplied from renewable energy sources such as wind or solar power, and hydrogen can also be sourced renewably such as from water electrolysis, solar thermal water splitting, or bioenergy, the overall plasma hydrogenation process could be CO_2 neutral and environmental-friendly.

Up until now, very limited research has concentrated on CO_2 hydrogenation using non-thermal plasmas, either with or without a catalyst.[33-42] The majority of this research reports CO as the dominant chemical, with CH_4 formed as a minor product and no CH_3OH detected.[35-36,40-42] In the late 90s, Eliasson and co-workers investigated CO_2 hydrogenation to CH_3OH using a dielectric barrier discharge (DBD). However, only trace amounts of CH_3OH were produced, with a maximum CH_3OH yield of 0.2% obtained at atmospheric pressure (1 bar), a relatively high plasma power of 400 W, a total flow rate of 250 ml/min and a H_2/CO_2 molar ratio of 3:1.[43] They also found that packing a $Cu/ZnO/Al_2O_3$ catalyst (a commercial methanol synthesis catalyst) in the discharge increased the methanol yield (from 0.1 to 1.0%), methanol selectivity (from 0.4 to 10.0%) and CO_2 conversion (from 12.4 to 14.0%) at a higher pressure (8 bar) under similar operating conditions.[37] However, the methanol yield and selectivity were still significantly lower than those reported in catalytic CO_2 hydrogenation processes. Recently, the formation of trace CH_3OH in plasma CO_2 reduction was also reported using a RF impulse discharge at low pressures (1-10 Torr).[38] Compared to catalytic CO_2 hydrogenation to methanol which has been carried out using a wide range of catalysts, a very limited number of catalysts have been examined in the plasma hydrogenation of CO_2. The knowledge for selecting efficient and appropriate catalysts for this reaction does not exist, whilst the influence of a catalyst on plasma hydrogenation of CO_2 is largely unknown. Significant pioneering works are required to explore the low temperature synthesis of methanol from CO_2 hydrogenation using non-thermal plasmas

at atmospheric pressure and to enhance the selectivity and yield of methanol through the development of novel reactor concepts and catalytic materials with high reactivity and stability.

In this study, we have developed a plasma-driven catalytic process for the synthesis of methanol with high selectivity from CO_2 hydrogenation at room temperature and atmospheric pressure for the first time (Scheme 2). Different reactor structures, including a unique DBD plasma system that uses water as a ground electrode, have been evaluated for the plasma hydrogenation of CO_2 in terms of the conversion of CO_2 and the concentration, selectivity and yield of products (CO, CH_4, methanol and ethanol). In addition, the role of H_2/CO_2 molar ratio and catalyst ($Cu/\gamma\text{-}Al_2O_3$ and $Pt/\gamma\text{-}Al_2O_3$) in the plasma hydrogenation process were investigated in the DBD reactor using a special water electrode. The Cu catalysts was chosen due to its high activity towards CH_3OH formation, whilst the noble metal Pt was selected due to its high capacity for H_2 dissociation and enhanced activity at low reaction temperature in comparison with non-noble metal catalysts. The maximum methanol yield of 11.3% and methanol selectivity of 53.7% were achieved when placing the $Cu/\gamma\text{-}Al_2O_3$ catalyst in the plasma, which is by far the highest methanol yield and selectivity reported in the plasma CO_2 hydrogenation process. The possible reaction pathways in the plasma hydrogenation of CO_2 to methanol with or without a catalyst were proposed by combined means of optical and electrical diagnostics, plasma kinetic modeling, product analysis and a range of catalyst characterization.

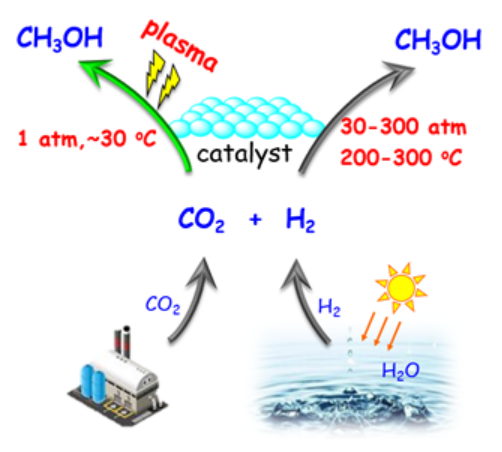

Scheme 2. Scheme of CO_2 hydrogenation to methanol.

EXPERIMENTAL SECTION

Experimental setup. Plasma hydrogenation of CO_2 was carried out using different DBD reactors at atmospheric pressure (Scheme 3, Scheme S1 and Table S1). Reactor I was a typical cylindrical DBD reactor using a stainless-steel rod (2 mm o.d.) as a high voltage electrode placed along the axis of a glass cylinder (10 mm o.d. × 8 mm i.d.), which was used as a dielectric. An aluminum foil sheet covered the outside of the glass cylinder and served as a ground electrode. Differing to reactor I, reactors II and III consisted of a pair of coaxial glass cylinders with water circulating in the space between the inner and outer cylinders, which acted as a ground water electrode. This specially designed water electrode is unique and could effectively remove heat generated by the discharge and maintain the reaction at room temperature. Reactor II was a typical double dielectric barrier discharge reactor as the high voltage electrode was covered by a quartz tube, while in reactor III the high voltage electrode was directly placed in the axis of the coaxial glass tube, same as the configuration used in reactor I. The discharge length of all the DBD reactors was 45 mm with a discharge gap of 3 mm. In the plasma-catalyst coupling mode, 3 g of catalyst was fully packed into the discharge area. A mixture of H_2 and CO_2 was fed into

the DBD reactor at a total flow rate of 40 ml/min. The DBD reactor was connected to an AC high voltage power supply with a peak voltage of up to 30 kV and a variable frequency of 7-12 kHz. In this work, the frequency of the power supply was fixed at 9 kHz. The electrical signals (applied voltage, current and voltage on the external capacitor) were recorded by a four-channel digital oscilloscope (Tektronix, MDO 3024). The discharge power was calculated by using the Q-U Lissajous method and was fixed at 10 W in this work.

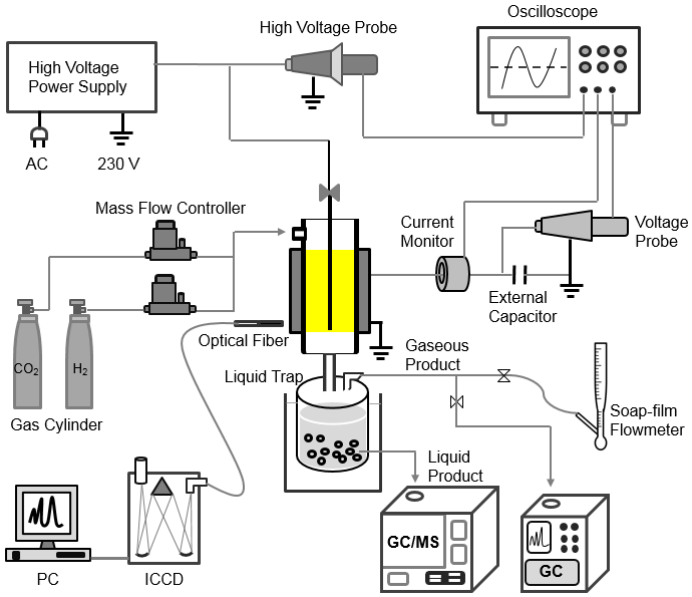

Scheme 3. Schematic diagram of experimental setup.

The gaseous products were analyzed using a gas chromatograph (Shimadzu GC-2014) equipped with a thermal conductivity detector (TCD) and a flame ionized detector (FID). A water/ice mixture bath was placed at the exit of the DBD reactor to condense liquid products. The oxygenates were qualitatively analyzed using a gas chromatography-mass spectrometer (GC-MS, Agilent GC 7820A and Agilent MSD 5973) and quantitatively analyzed using a gas chromatograph (Agilent 7820) equipped with a FID with a DB-WAX column. The change of the

gas volume before and after the reaction was measured using a soap-film flowmeter (Scheme 3). Sampling and measurements started after running the reaction for 1.5 hours.

To evaluate the reaction performance of CO_2 hydrogenation to methanol, the concentration of major products (methanol and ethanol) in the condensate was calculated via corresponding formula of standard calibrated concentration curves (Table S2).

The conversion of CO_2 is defined as:

$$X_{CO_2}\ (\%) = \frac{\text{moles of } CO_2 \text{ converted}}{\text{moles of initial } CO_2} \times 100 \quad (1)$$

The selectivity of gaseous products can be calculated:

$$S_{CO}\ (\%) = \frac{\text{moles of CO produced}}{\text{moles of } CO_2 \text{ converted}} \times 100 \quad (2)$$

$$S_{CH_4}\ (\%) = \frac{\text{moles of } CH_4 \text{ produced}}{\text{moles of } CO_2 \text{ converted}} \times 100 \quad (3)$$

The selectivity of the liquid products can be calculated:

$$\text{The total selectivity of liquid products } (\%) = 100\% - \left(S_{CO} + S_{CH_4}\right) \quad (4)$$

The selectivity of $C_xH_yO_z$ can be calculated:

$$S_{C_xH_yO_z}\ (\%) = \text{carbon of } C_xH_yO_z \text{ (mol \%) in the liquid product} \times (4) \quad (5)$$

The yield of $C_xH_yO_z$ can be calculated:

$$Y_{C_xH_yO_z}\ (\%) = S_{C_xH_yO_z}\ (\%) \times X_{CO_2}\ (\%) \quad (6)$$

The energy efficiency of methanol formation (mmol/kWh) is defined as:

$$\text{Energy efficiency} = \frac{\text{moles of methanol produced (mmol/min)}}{\text{discharge power (kW)}} \quad (7)$$

Catalyst preparation. Both catalysts were synthesized by incipient wetness impregnation over as-is commercially obtained γ-Al_2O_3 (Dalian Luming Nanometer Material Co., Ltd.) using a hydrothermal method. Metal precursor solution was prepared by dissolving each metal salt in water, which was just sufficient to fill the pores of 8 g of the support. The γ-Al_2O_3 support was firstly calcined at 400 ^oC for 5 h to remove impurities (e.g., adsorbed H_2O), then the support was added to the precursor solution and stirred until it was thoroughly mixed. The resulting mixture was successively kept at room temperature for 3 h, vacuum freeze-dried overnight at -50 ^oC and dried in air at 120 ^oC for 5 h. The dried sample (20-40 mesh) was finally calcined in a pure argon DBD plasma (reactor I) at around 350 ^oC for 3 h with an argon flow rate of 80 ml/min. The metal loading of the Pt and Cu catalysts was ca. 1 wt.% and ca. 15 wt.%, respectively.

Catalyst characterization. The metal-support interaction was evaluated by H_2 temperature-programmed reduction (H_2-TPR) using a Quantachrome ChemBET 3000 Chemisorption instrument. The sample (100 mg) was pretreated at 500 ^oC for 1 h in a He flow (20 ml/min), and then cooled to 50 ^oC. The pre-treated sample was exposed to a H_2/He mixture (10 vol.% H_2) and was heated from 150 to 800 ^oC at a constant heating rate of 14 ^oC/min to create the TPR profile.

X-ray diffraction (XRD) patterns of the catalysts before and after the reaction were recorded using a Rigaku D-Max 2400 X-ray diffractometer with Cu-K_α radiation. Transmission electron microcopy (TEM) was used to characterize metal particles formed on the catalyst surface using a JEOL 2010 with EDS of Oxford Instruments INCA energy system at an accelerating voltage of 200 kV.

Optical emission spectroscopic (OES) diagnostics. The emission spectra of the H_2/CO_2 discharges were recorded using a Princeton Instruments ICCD spectrometer (SP 2758) in the range of 200-1200 nm via an optical fiber, placed close to the ground electrode of the DBD

reactors. The slit width of the spectrometer was fixed at 20 μm, while a 300 g mm^{-1} grating was used for these measurements.

RESULTS

Effect of reactor design on plasma CO_2 hydrogenation. Figure 1 shows the structure of the DBD reactors significantly affects the performance of plasma CO_2 hydrogenation. Methanol and ethanol were identified as the major oxygenates in this process, while CO and CH_4 were the major gas products. Interestingly, the conversion of CO_2 was similar (10-14%) when using the different DBD reactors. However, the distribution of gas and liquid products was strongly dependent on the structure of the DBD reactors. Clearly, compared to reactor I and II, more methanol was produced when using reactor III. Reactor I showed the lowest methanol formation, but the highest selectivity of the by-product CO (Figure 1a and 1b). Compared with reactor I, reactor III using water as the ground electrode instead of the aluminum foil sheet resulted in a significant increase of CH_3OH concentration by a factor of 37 (from 0.1 to 3.7 mmol/L, Figure 1a), a dramatic increase of CH_3OH selectivity by a factor of 54 (from 1.0 to 54.2%, Figure 1b) and CH_3OH yield by a factor of 71 (from 0.1 to 7.1%, Figure 1c), while the CO selectivity (30.4%) obtained using reactor III was significantly lower than that (87.2%) using reactor I, even though the CO_2 conversion was maintained at ~13% in both cases. Compared to reactor III, the use of a high voltage electrode covered by a quartz tube in reactor II decreased the reaction performance of the plasma hydrogenation process in terms of the concentration, selectivity and yield of oxygenates whilst still keeping a similar CO_2 conversion. Clearly, reactor III showed the best performance towards the synthesis of oxygenates (methanol and ethanol) from CO_2 hydrogenation, thus it was selected for the following experiments.

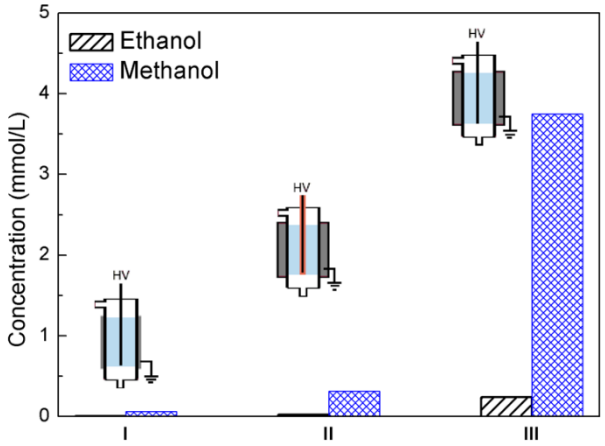
Ethanol
Methanol
Concentration (mmol/L)
HV
HV
HV
I
II
III

(a)

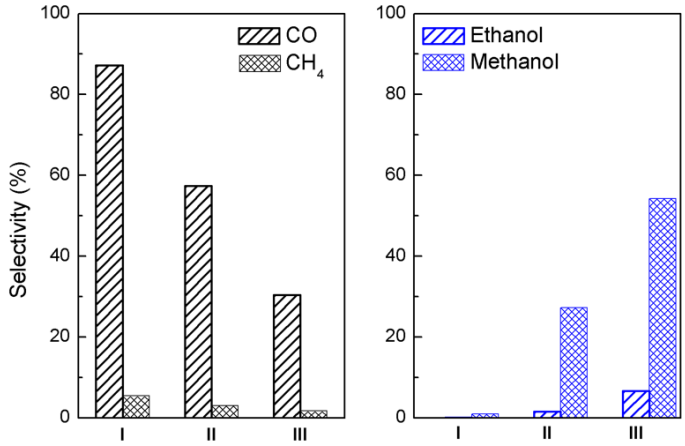
CO
CH4
Selectivity (%)
Ethanol
Methanol
I
II
III

(b)

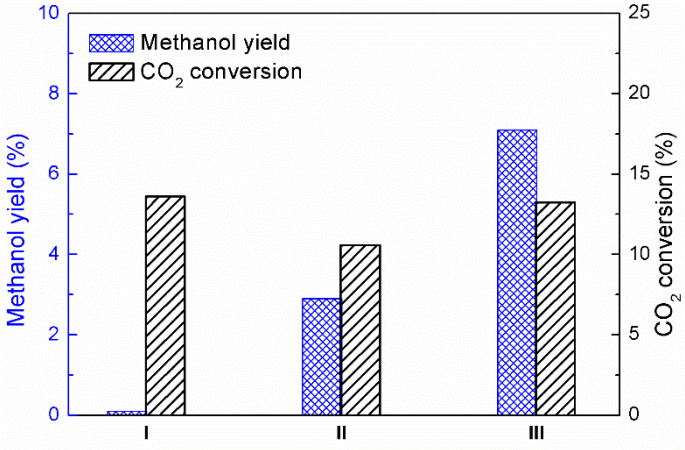
Methanol yield
CO2 conversion
Methanol yield (%)
CO2 conversion (%)
I
II
III

(c)

Figure 1. Influence of reactor structure (reactor I, II and III) on the reaction performance of the plasma hydrogenation process: (a) concentration of oxygenates; (b) selectivity of gas products and oxygenates; (c) methanol yield and CO_2 conversion (reaction pressure 1 atm, H_2/CO_2 molar ratio 3:1. More details about the reactor structures can be found in Scheme S1 and Table S1).

Effect of H_2/CO_2 molar ratio and catalyst. The concentration and yield of CH_3OH, as well as the conversion of CO_2 were affected by the H_2/CO_2 molar ratio and especially by the catalysts, (Figure 2a and 2b), while the corresponding selectivity of CH_3OH varied slightly in the range of 50-60% (Figure 2c). Increasing the H_2/CO_2 molar ratio from 1:1 to 3:1 increased the concentration and yield of CH_3OH from 1.7 to 3.7 mmol/L and 6.0 to 7.2%, respectively (Figure 2a and 2b), while the selectivity of CO decreased from 40.0 to 30.0% with the increase of the H_2/CO_2 molar ratio (Figure 2c).

In addition, the Cu/γ-Al_2O_3 and Pt/γ-Al_2O_3 catalysts were also evaluated in the plasma-catalytic hydrogenation of CO_2 to methanol, as Cu and Pt typically have high activity towards methanol synthesis and H_2 dissociation, respectively. Clearly, packing the catalysts into the plasma significantly enhanced the reaction performance (e.g. concentration and yield of methanol), but also increased the formation of by-product CO. The Cu/γ-Al_2O_3 catalyst exhibited a similar selectivity but much better activity towards CH_3OH formation compared to the Pt/γ-Al_2O_3 catalyst (Figure 2). At the H_2/CO_2 molar ratio of 3:1, compared to the plasma hydrogenation without a catalyst, placing the Cu/γ-Al_2O_3 catalyst in the plasma discharge significantly increased the CH_3OH concentration by a factor of ~7 (from 3.7 to 25.6 mmol/L) and enhanced the CH_3OH yield (from 7.2 to 11.3%) and CO_2 conversion (from 13.2 to 21.2%), whist maintaining the CH_3OH selectivity at a similar level of around 54.0%. In addition, the

performance of this process was stable after 6 hours continuous running over the Cu/γ-Al_2O_3 catalyst.

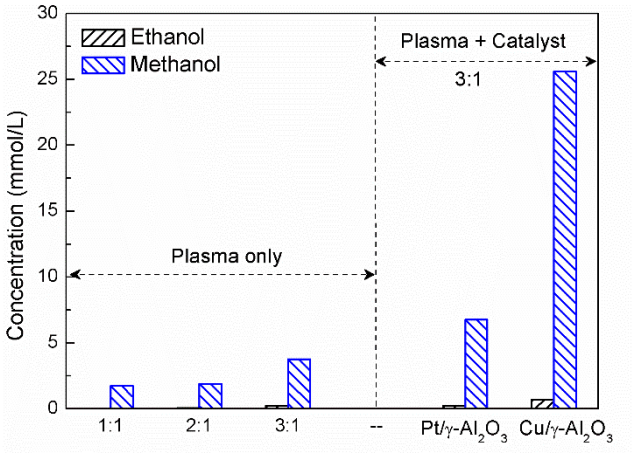

(a)

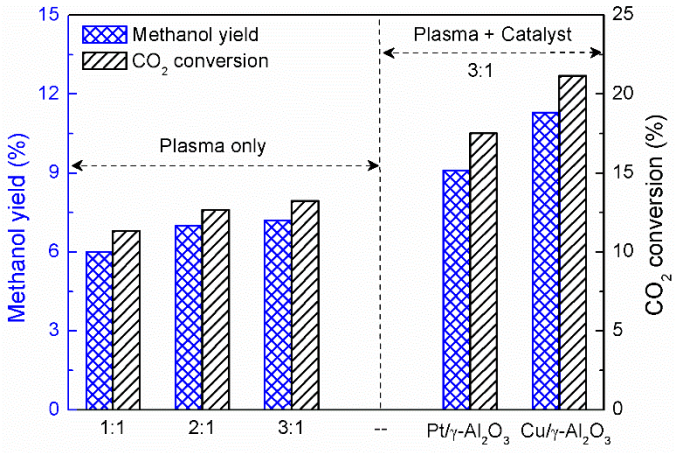

(b)

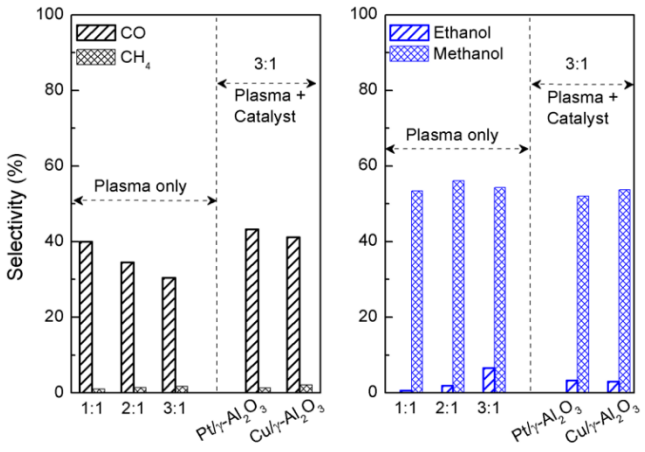

(c)

Figure 2. Effect of H_2/CO_2 molar ratio and catalysts on the reaction performance of the plasma hydrogenation process: (a) concentration of oxygenates; (b) selectivity of gas products and oxygenates; (c) methanol yield and CO_2 conversion.

The energy efficiency of methanol production in the plasma CO_2 hydrogenation was also strongly dependent on the structure of the DBD reactors and catalyst composition, as shown in Figure S1. The combination of plasma with the Cu/γ-Al_2O_3 catalyst using reactor III showed the highest energy efficiency of 306 mmol/kWh for methanol formation, about 84 times higher than that achieved using reactor I only (3.6 mmol/kWh).

Catalyst properties. The physicochemical properties of γ-Al_2O_3 and as-synthesized catalysts were examined using a range of catalyst characterization techniques including XRD, TEM and H_2-TPR. The γ-Al_2O_3 support used here was a crystalline material (Figure 3) with a Brunauer-Emmett-Teller (BET) surface area of 114.8 m^2/g. The TEM images of the catalysts showed that the Cu and Pt nanoparticles (NPs) were highly dispersed on the surface of the γ-Al_2O_3 support (Figure 4). The average size of Cu NPs was approx. 10 nm, larger than that of Pt NPs (<5 nm). The XRD analysis of as-synthesized catalysts revealed that Cu existed in the form of CuO over

the γ-Al_2O_3 support, while metallic Cu was found to be the major phase composition of the Cu catalyst after the plasma CO_2 hydrogenation (Figure S2). No obvious diffraction peaks of Pt were identified in the XRD pattern of the Pt/γ-Al_2O_3 catalyst (Figure 3), indicating a high dispersion of Pt NPs with small particle sizes on the surface of the Pt/γ-Al_2O_3 catalyst, also confirmed by the TEM results. The H_2-TPR analysis of the catalysts revealed that the reduction of the CuO/γ-Al_2O_3 catalyst occurred in the low temperature range of 150-300 ^oC (Figure 5). By contrast, the TPR spectrum of the Pt/γ-Al_2O_3 catalyst showed a few negative peaks with no reduction peak, which suggested that Pt metallic state was formed on the γ-Al_2O_3 support after the Ar plasma calcination. Similar findings were reported by Liu et al. that argon plasmas are effective for the reduction and calcination of supported noble metal catalysts at low temperature even in the absence of hydrogen, while it is difficult to convert Cu precursor (e.g. Cu salts) to metallic Cu using an argon plasma treatment without hydrogen.[44] The XRD pattern of pure γ-Al_2O_3 indicated that these negative peaks seen in the TPR of the Pt/γ-Al_2O_3 catalyst were not from γ-Al_2O_3, but might be attributed to the decomposition of Pt-H_x species formed through hydrogen adsorption and diffusion on the Pt/γ-Al_2O_3 catalyst.[45-46]

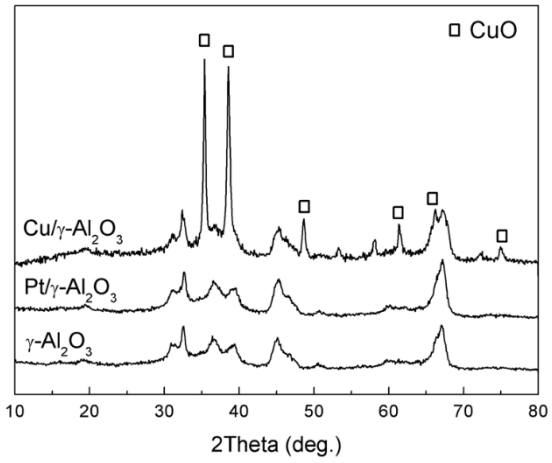

Figure 3. XRD patterns of as-synthesized catalysts

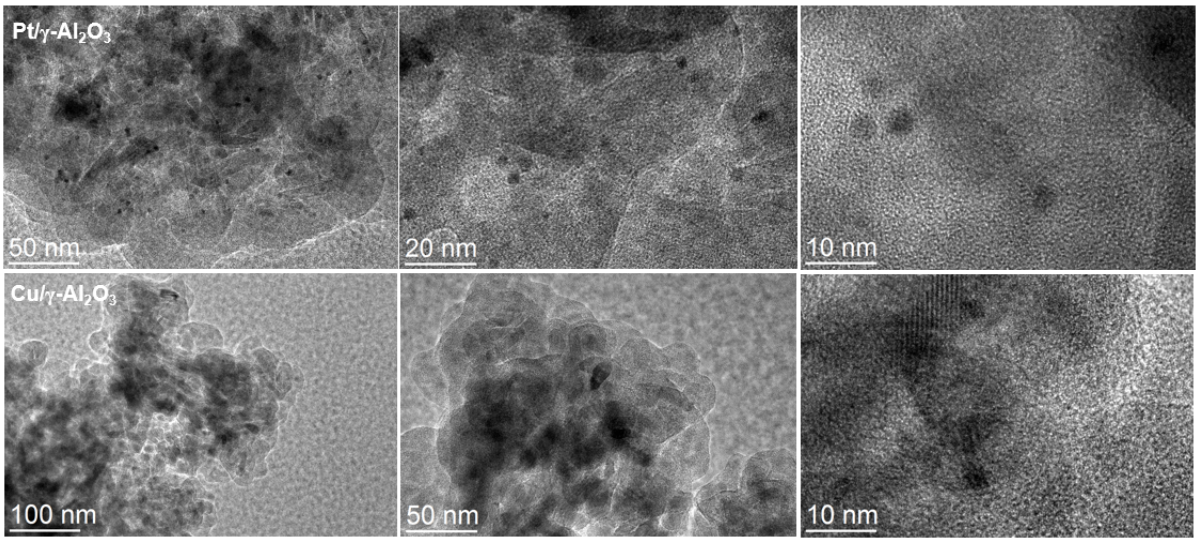

Figure 4. TEM images of Cu/γ-Al_2O_3 and Pt/γ-Al_2O_3 catalysts.

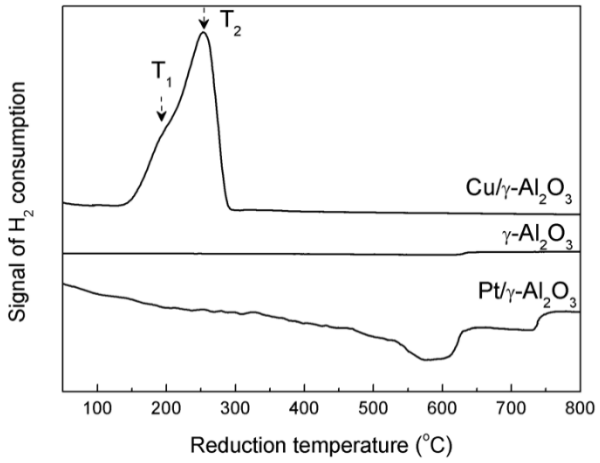

Figure 5. TPR profiles of as-synthesized catalysts (the signal attenuation of Cu/γ-Al_2O_3, γ-Al_2O_3 and Pt/γ-Al_2O_3 was 16, 16 and 1, respectively).

DISCUSSION

Plasma-driven CO_2 hydrogenation to methanol. In this work, room temperature and atmospheric pressure hydrogenation of CO_2 to methanol has been successfully achieved using a

DBD plasma reactor, even in the absence of a catalyst. The reaction performance of the plasma hydrogenation process strongly depended on the structure of the DBD reactor, while reactor III with a unique specially designed ground water electrode showed the highest methanol production (selectivity of 54.2%) and CO_2 conversion (Figure 1).

As shown in Figure 6, the discharge generated in reactor III was dominated by strong filaments, while the discharge formed in reactor II with a double dielectric structure was much weaker and more uniform, which is also evidenced by the different numbers and amplitudes of current pulses presented in Figure 7. However, the H_2/CO_2 discharge produced by different DBD reactors showed a similar emission spectrum (Figure 8), including CO Angstrom bands (451-608 nm, $B^1\sum \rightarrow A^1\prod$, band head at 519.4 nm), H_α (656.3 nm, $3d^2D \rightarrow 2p^2P^0$) and O atomic lines (777.5 nm, $3s^5S^0 \rightarrow 3p^5P$; 844.7 nm, $3s^3S^0 \rightarrow 3p^3P$), except for CO (674.7 nm, $a'^3\sum \rightarrow a^3\Pi$) which was only observed in reactor I. Notably, the relative intensity of H_α atomic line and CO band head (519.4 nm) was significantly different, with the H_α/CO intensity ratio of 3.6, 5.2 and 9.5 for reactor III, II and I, respectively, which indicated that CO_2 can be activated more easily in reactor III compared to the other two reactors as CO was only produced from CO_2. These findings agreed with the reaction performance of the plasma process presented in Figure 1. In addition, different reactor structures resulted in different plasma temperatures which play a key role in chemical reactions. Both reactor II and III have a special design of using water as the ground electrode, which effectively maintained the reaction temperature of the plasma hydrogenation at ~30 ^oC (Scheme S2). By contrast, the reaction temperature in the reactor I with an aluminum foil as the ground electrode was significantly higher (~350 ^oC). As CO_2 hydrogenation to methanol is an exothermic reaction, reactor II and III with lower operating temperatures offered a higher activity for the formation of oxygenates such as methanol and

ethanol (Figure 1). However, CO_2 hydrogenation using a DBD reactor (e.g. reactor I) at higher temperatures (e.g. 350 ^oC) tends to produce mainly CO rather than oxygenates, which can also be confirmed in our previous works.[42] Furthermore, low temperatures can inhibit further decomposition of produced oxygenates (e.g. methanol) in the plasma hydrogenation of CO_2, resulting in a higher methanol production. Our results suggest that discharge mode and reaction temperature are the key factors for the effective synthesis of oxygenates in a plasma-driven CO_2 hydrogenation process at atmospheric pressure (1 atm).

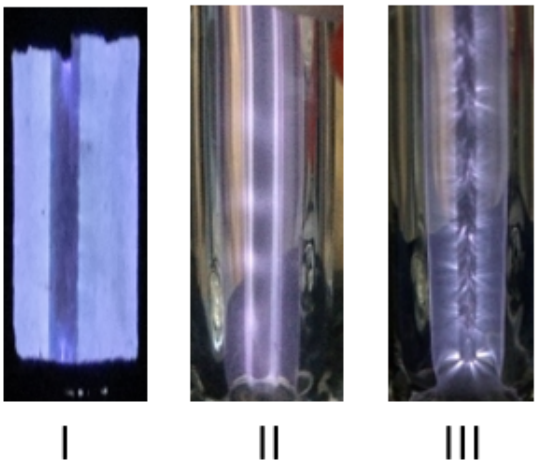

Figure 6. Images of H_2/CO_2 discharge generated in different DBD reactors (I, II and III) without a catalyst.

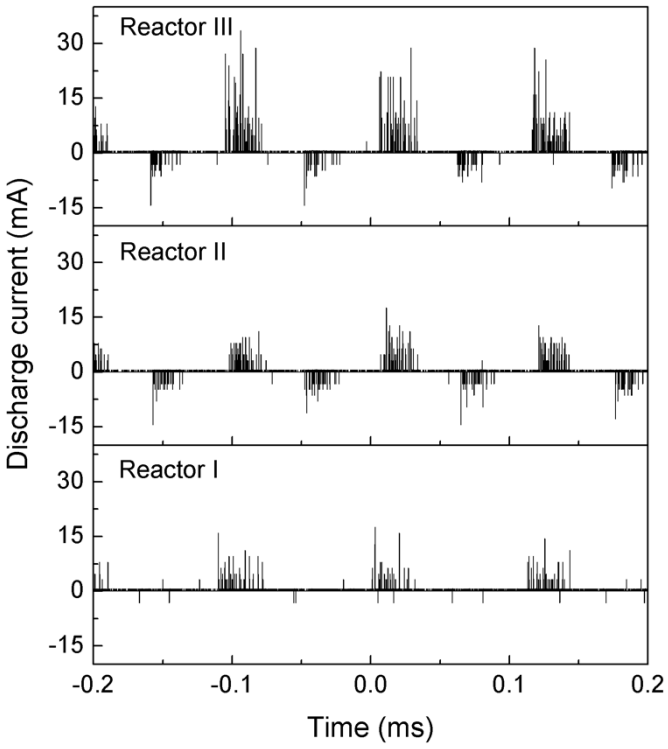

Figure 7. Current signals of H_2/CO_2 discharge using different DBD reactors.

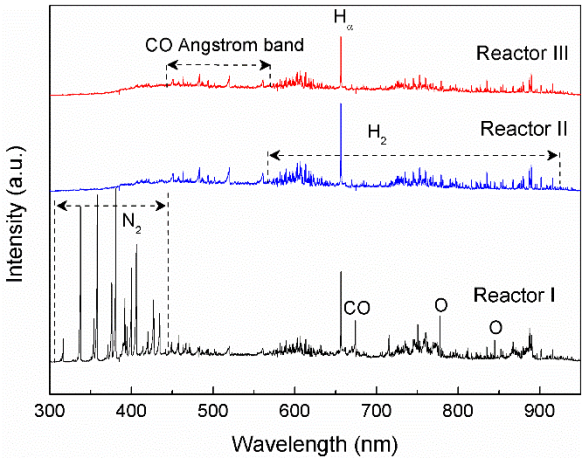

Figure 8. Emission spectra of H_2/CO_2 DBD using different reactor structures (H_2/CO_2 molar ratio 3:1, and 2 s exposure time. For reactor I, the N_2 molecular bands were generated due to the

interference of air, which existed between the ground electrode and the outer wall of the outer glass cylinder).

Scheme 4 presents the possible reaction pathways in the plasma hydrogenation of CO_2 to methanol without a catalyst. In the H_2/CO_2 DBD, the electron impact dissociation of CO_2 plays a key role in the production of CO as the density of ground state CO_2 is significantly higher than that of vibrationally excited CO_2 (Figure S3), while the electron impact vibrational excitation of CO_2 makes a minor contribution to CO_2 dissociation for the production of CO and O.[47] The electron impact dissociation of CO_2 in its vibrational excited states or ground state will most likely form CO in its ground state ($^1\sum$) and O atoms in both the ground state (^3P) and metastable state (^1D). However, since CO bands were observed in the emission spectra of the H_2/CO_2 discharge, CO could also be formed in excited states.[26]

The produced O radicals might further collide with part of $CO_2(v)$ molecules to produce CO (R4). Special attention was given to R5, although the reaction of ground state CO_2 with H radicals for CO production has a very low reaction rate coefficient of 1.4×10^{-29} cm^3 $molecule^{-1}s^{-1}$ and a high E_a of 111 kJ/mol at 300 K,[48] H radicals could react with vibrational excited CO_2 molecules to form CO. The vibrational energy of reagents is considered the most effective in overcoming the activation barriers of an endothermic reaction.[39,49] However, due to the relatively low density of vibrational excited CO_2 species present in the H_2/CO_2 DBD, the contribution of these reaction routes for CO formation could be insignificant. CO can be further hydrogenated to form HCO with a high reaction rate coefficient of 2.5×10^{-14} cm^3 $molecule^{-1}$ s^{-1} at 305 K via R6.[50] Subsequently, the recombination of HCO with itself forms H_2CO (R7),[51] followed by stepwise hydrogenation to generate methanol (R8, R9).[52-53] All of these reactions have a high reaction rate coefficient at 300 K (5.0×10^{-11}, 4.0×10^{-14} and 3.4×10^{-10} cm^3 $molecule^{-1}$ s^{-1} for R7, R8 and R9,

respectively). However, HCO + H → CO + H_2 is a competitive reaction to consume HCO (6.64×10^{-11} cm^3 $molecule^{-1}$ s^{-1}, 298 K),[54] which can significantly weaken the formation of H_2CO (R7) since the former reaction has a similar reaction rate coefficient as that of R7. Although HCO hydrogenation can also produce H_2CO, i.e., HCO + H → H_2CO (3.5×10^{-13} cm^3 $molecule^{-1}$ s^{-1} at 1500 K),[55] HCO + H_2 → H_2CO + H (2.7×10^{-26} cm^3 $molecule^{-1}$ s^{-1} at 300 K),[48] their contributions to the synthesis of methanol could be neglected due to very low reaction rate coefficients. Therefore, the performance of the plasma CO_2 hydrogenation to methanol could be limited mainly by the formation of H_2CO in this study (Scheme 4).

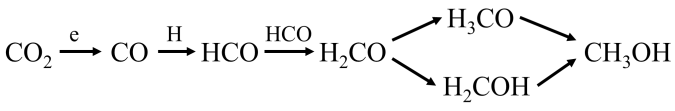

Scheme 4. Possible reaction pathways for methanol production in the plasma hydrogenation of CO_2 without a catalyst.

$CO_2(v) + O \rightarrow CO + O_2$ (R4)

$CO_2(v) + H \rightarrow OH + CO$ (R5)

$CO + H \rightarrow HCO$ (R6)

$HCO + HCO \rightarrow H_2CO + CO$ (R7)

$H_2CO + H \rightarrow H_3CO$ (R8)

$H_3CO + H \rightarrow CH_3OH$ (R9)

Plasma-catalytic hydrogenation of CO_2 to methanol. The combination of DBD with the catalysts significantly enhanced the production of methanol (yield and concentration) and CO_2 conversion, and slightly changed the selectivity of methanol (Figure 2), indicating the existence of plasma-assisted surface reactions in addition to the gas phase reactions. Compared to the

plasma reaction without a catalyst, the presence of the catalyst in the plasma-catalytic CO_2 hydrogenation offers new reaction routes for chemical reactions. Interestingly, the emission spectra of the discharge with and without the catalyst were completely different (Figure 9). Compared to the plasma process without a catalyst, placing the Cu or Pt catalyst in the discharge significantly decreased the intensity of H_α atomic line, while the CO Angstrom bands and H_2 bands almost vanished in the plasma-catalytic process. Similar findings were also reported in previous works.[56] This phenomenon could be attributed to the adsorption of gas phase species (e.g. CO) onto the surface of the catalysts. In addition, the formation of weak filamentary discharge resulting from the transition of the discharge mode in the presence of the catalyst might also lead to the decreased emission intensity.

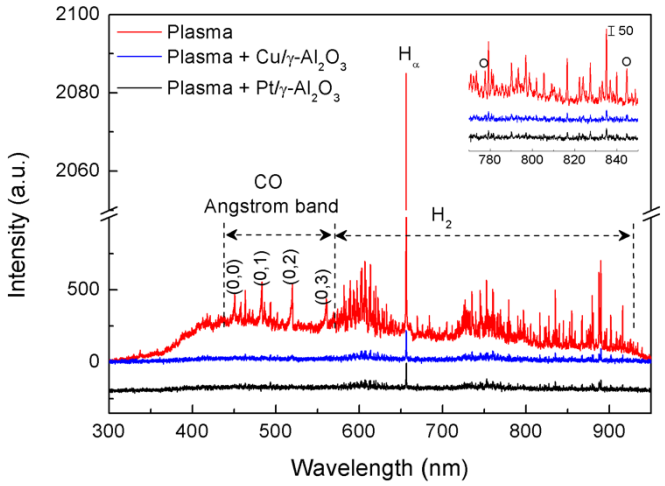

Figure 9. Emission spectra of H_2/CO_2 DBD with different packing catalysts (H_2/CO_2 molar ratio 3:1, 2 s exposure time).

Compared to catalytic CO_2 hydrogenation without using a plasma, in the hybrid plasma-catalytic hydrogenation process, plasma can activate CO_2 and H_2 and produce a variety of

chemically reactive species including radicals, excited atoms, ions and molecules such as CO_2(v), CO, H and O radicals. These energetic species which are produced at a relatively low temperature are capable of initiating a range of gas phase and surface reactions. Another significant advantage of coupling a catalyst with a plasma system comes from the increased reaction time of reactants and hence improved yield of products, resulting from the adsorption of the reactants onto the surface and the selective adsorption of some species.[57] Scheme 5 shows the possible major reactions for methanol generation on catalyst surfaces in the plasma-catalytic CO_2 hydrogenation process, given the mechanisms of catalytic CO_2 hydrogenation to methanol.[3-5, 12, 58,59] Plasma-created radicals in the boundary layer near the catalyst surfaces can be adsorbed directly and it is likely that this will require a much lower energy.[57,60,61] Firstly, CO formed in the plasma gas phase reactions can be directly adsorbed onto the catalyst surface, which is unique in the plasma-catalytic CO_2 hydrogenation process, followed by stepwise hydrogenation towards the formation of methanol with $HCO_{(ad)}$, $H_2CO_{(ad)}$ and $H_3CO_{(ad)}$ (or $H_2COH_{(ad)}$) being the adsorbed intermediates.[12,20-21,58] Note that reactions can take place between species adsorbed onto the catalytic surface with either other adsorbed species or with gas phase species near the catalyst surface. In addition to the adsorption of ground state CO_2, CO_2(v) could be adsorbed onto the catalyst surface although the excited species are more likely to be quenched or relaxed by the surface. The initial hydrogenation of $CO_{2(ad)}$ can generate formate (HCOO), which undergoes a series of hydrogenation and dissociation reactions to form CH_3OH, as shown in Scheme 5. The conversion of CO_2 to CH_3OH via the formate pathways can be limited by the formation of $HCOO_{(ad)}$ and/or the hydrogenation of $HCOOH_{(ad)}$ to $H_2COOH_{(ad)}$, which are highly activated processes. [59] In addition, methanol can be synthesized via RWGS + CO-Hydro pathways on the catalyst surfaces. The hydrogenation of $CO_{2(ad)}$ forms HOCO(ad) initially,

followed by the dissociation of $HOCO_{(ad)}$ to form $CO_{(ad)}$ and $OH_{(ad)}$. The produced $CO_{(ad)}$ can either desorb or convert to methanol via stepwise hydrogenation reactions. Previous theoretical studies have shown that CO_2 activation on Pt NPs prefers the hydrogenation reaction to form $HOCO_{(ad)}$ initially, which suggests that CO_2 hydrogenation is likely to prefer the RWGS + CO-Hydro pathways rather than the format pathways on the Pt NPs. [59]

Molecule adsorption is not a spontaneous process, mainly depending on the interaction potential of the molecule-catalyst system. Compared to ground state CO_2, the adsorption of $CO_2(v)$ is energetically preferred due to its higher internal energy, [62] although this contribution to the enhanced adsorption process depends on the plasma properties (e.g. electric field, electron energy) and could be minor in this process. Previous works reported the enhanced adsorption of vibrational excited CH_4 species on Ni metal surfaces was the origin of the improved CH_4 conversion in plasma-catalytic steam reforming of methane compared to the thermal catalytic process (50% in plasma-catalysis versus 20% in thermal catalysis) at 400 ^{o}C.[63] Furthermore, when $CO_2(v)$ is adsorbed onto the catalyst surface, the energy of $CO_2(v)$ can be rapidly dissipated into the catalyst by the formation of low-energy electron-hole pairs and Auger de-excitation,[64] which could change the physicochemical properties (i.e. electronic structure) of the catalyst and make it active, triggering the hydrogenation of $CO_{2(ad)}$ to form $HCOO_{(ad)}$ or $HOCO_{(ad)}$. In addition, $CO_{2(ad)}$ can also generate $CO_{(ad)}$ through the reverse water gas shift reaction on the catalyst surfaces,[3] which explains the increased CO formation when packing the catalysts in the plasma reactors (Figure 2). The presence of a range of reactive species in the plasma-catalytic process is crucial for CO_2 hydrogenation to methanol on the catalyst surface at ambient conditions. Clearly, more reaction routes for the production of methanol could be

initiated when placing the catalysts in the plasma, which significantly enhanced the generation of methanol in the plasma-catalytic process.

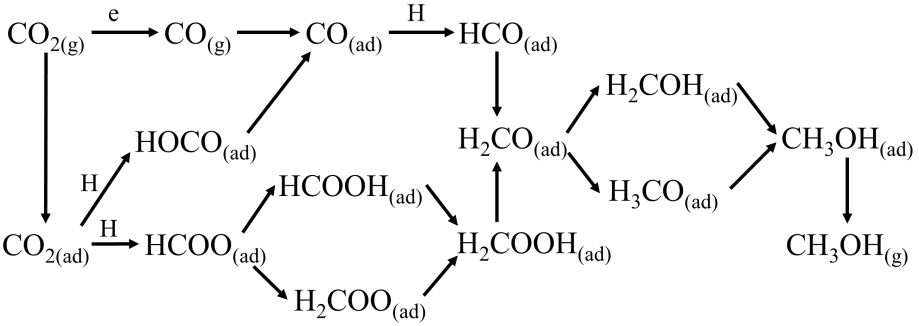

Scheme 5. Possible reaction pathways on catalyst surfaces in the plasma-catalytic CO_2 hydrogenation to methanol.

Although packing the Cu/γ-Al_2O_3 or Pt/γ-Al_2O_3 catalysts into the plasma both increased methanol production (e.g. methanol yield), the Cu/γ-Al_2O_3 catalyst showed a better reaction performance in the plasma-catalytic hydrogenation process (Figure 2). The OES diagnostics showed that the catalysts had almost no effect on the emission spectra of the H_2/CO_2 discharges (Figure 9), suggesting that the physicochemical properties of the catalysts might be more important for determining the different reaction performances in the plasma-catalytic hydrogenation process. The average size of Cu NPs of the Cu/γ-Al_2O_3 catalyst was much larger than that of the Pt/γ-Al_2O_3 catalyst (Figure 4), but the Cu catalyst showed a higher reaction performance in terms of methanol selectivity and yield compared to the Pt catalyst, which suggests that the particle size of these catalysts might not be the determining factor affecting methanol synthesis. The XRD pattern of the spent Cu catalyst showed that metallic Cu was the major phase composition over the catalyst surface, which is very active for CO_2 hydrogenation to methanol. Recently, Studt et al. reported that the reaction performance of CO_2 hydrogenation to methanol is closely related to the oxygen adsorption energy (ΔE_O) of intermediates formed on a

metal surface. The proposed theoretical activity volcano for CO_2 hydrogenation to methanol showed that those elements located at the top of the volcano with a moderate ΔE_O favor this reaction.[22] They found that elemental copper is closest to the top of the volcano at atmospheric pressure and binds moderately to the intermediates of CO_2 hydrogenation,[22] which could explain why the Cu catalyst had a better performance for methanol synthesis compared to the Pt catalyst. More recently, Kattle et al investigated the mechanisms of CO_2 hydrogenation on Pt NPs over Pt/SiO_2 and Pt/TiO_2 catalysts. They found that Pt NPs alone cannot catalyze the reaction due to the weak CO_2 binding on the catalysts. Once the CO_2 is stabilized, the hydrogenation of CO_2 to CO through the reverse water gas shift reaction is promoted.[59] Ferri et al. found that CO_2 was adsorbed on γ-Al_2O_3 of a Pt/γ-Al_2O_3 catalyst to form carbonate-like species, which further reacted with hydrogen to generate CO as the final product, using in-situ attenuated total reflection infrared (ATR-IR) spectroscopy.[65] These findings could explain why the presence of the Pt/γ-Al_2O_3 catalyst in the plasma CO_2 hydrogenation process gave a higher CO selectivity compared to the plasma hydrogenation without a catalyst or when using the Cu catalyst (Figure 2). These results show that the interaction of reaction intermediates with catalyst surfaces is also crucial in the plasma-catalytic CO_2 hydrogenation to methanol.

CONCLUSION

CO_2 hydrogenation to methanol with a high selectivity has been successfully achieved at atmospheric pressure and room temperature (~30 ^oC) using a specially designed water-cooled DBD reactor. The reaction performance of the plasma hydrogenation process was strongly dependent on the design and structure of the plasma reactors and the catalysts, while the influence of H_2/CO_2 molar ratio on the reaction was less critical. Reactor III, which featured a

unique water electrode design, showed the highest production of methanol. Compared to the plasma hydrogenation of CO_2 without a catalyst, packing the catalysts into the plasma process significantly enhanced the conversion of CO_2 and the concentration and yield of methanol, with a slight change in methanol selectivity. Compared to the Pt/γ-Al_2O_3 catalyst, the Cu/γ-Al_2O_3 catalyst showed a better activity towards methanol synthesis in the plasma process. The optimal methanol yield of 11.3% and methanol selectivity of 53. 7% were achieved over the Cu/γ-Al_2O_3 catalyst using reactor III at a stoichiometric feed, atmospheric pressure (1 atm) and room temperature, which is by far the highest performance (methanol selectivity and yield) reported in plasma hydrogenation of CO_2. More importantly, the coupling of the plasma and catalysts enables selective catalytic CO_2 hydrogenation (to methanol) to occur at room temperature and atmospheric pressure, providing a new alternative approach that lowers the kinetic barrier and energy cost of catalytic CO_2 hydrogenation for methanol synthesis instead of using traditional approaches, e.g., higher reaction temperature and higher pressure. This unique plasma process opens a new route for the conversion of low value feedstock (CO_2) to commodity liquid fuels and platform chemicals (e.g. methanol) at ambient conditions with reduced energy consumption, and has significant potential to deliver a step change in future CO_2 utilization and radically transform the chemical and energy industry.

ASSOCIATED CONTENT

Supporting Information

The Supporting Information is available free of charge on the ACS Publications website at DOI: XXX.

Structure of different DBD reactors, formula of standard concentration curves, energy efficiency of methanol synthesis, measurement of reaction temperature, and plasma chemical modeling.

AUTHOR INFORMATION

Corresponding Author

* Xin Tu. E-mail: xin.tu@liverpool.ac.uk; xin.tu@liv.ac.uk

ORCID

Xin Tu: 0000-0002-6376-0897

Present Addresses

† Department of Electrical Engineering and Electronics, University of Liverpool, Liverpool, L69 3GJ, UK.

ACKNOWLEDGEMENTS

The support of this work by the UK EPSRC SUPERGEN Hydrogen & Fuel Cell (H2FC) Hub (EP/J016454/1) ECR Project (Ref. No. EACPR_PS5768) is gratefully acknowledged.

REFERENCES

1. Roadmap 2050 – A Practical Guide to a Prosperous Low-Carbon Europe, EU, **2010**.
2. Koornneef, J.; Ramirez, A.; Turkenburg, W.; Faaij, A., *Prog. Energy Combust. Sci.* **2012,** *38*, 62-86.
3. Porosoff, M. D.; Yan, B.; Chen, J. G., *Energy Environ. Sci.* **2016,** *9*, 62-73.
4. Wang, W.; Wang, S.; Ma, X.; Gong, J., *Chem. Soc. Rev.* **2011,** *40*, 3703-3727.
5. Liu, P.; Yang, Y.; White, M. G., *Surf. Sci. Rep.* **2013,** *68*, 233-272.
6. Jadhav, S. G.; Vaidya, P. D.; Bhanage, B. M.; Joshi, J. B., *Chem. Eng. Res. Des.* **2014,** *92*, 2557-2567.

7. Kattel, S.; Yan, B.; Yang, Y.; Chen, J. G.; Liu, P., *J. Am. Chem. Soc.* **2016,** *138*, 12440-12450.
8. Xiao, S.; Zhang, Y.; Gao, P.; Zhong, L.; Li, X.; Zhang, Z.; Wang, H.; Wei, W.; Sun, Y., *Catal. Today* **2017,** *281*, 327-336.
9. Witoon, T.; Kachaban, N.; Donphai, W.; Kidkhunthod, P.; Faungnawakij, K.; Chareonpanich, M.; Limtrakul, J., *Energy Convers. Manag.* **2016,** *118*, 21-31.
10. Senanayake, S. D.; Ramirez, P. J.; Waluyo, I.; Kundu, S.; Mudiyanselage, K.; Liu, Z.; Liu, Z.; Axnanda, S.; Stacchiola, D. J.; Evans, J., *J. Phys. Chem. C* **2016,** *120*, 1778-1784.
11. Gaikwad, R.; Bansode, A.; Urakawa, A., *J. Catal.* **2016,** *343*, 127-132.
12. Behrens, M.; Studt, F.; Kasatkin, I.; Kühl, S.; Hävecker, M.; Abild-Pedersen, F.; Zander, S.; Girgsdies, F.; Kurr, P.; Kniep, B.-L., *Science* **2012,** *336*, 893-897.
13. Fichtl, M. B.; Schumann, J.; Kasatkin, I.; Jacobsen, N.; Behrens, M.; Schl gl, R.; Muhler, M.; Hinrichsen, O., *Angew. Chem. Int. Ed.* **2014,** *53*, 7043-7047.
14. Kuld, S.; Thorhauge, M.; Falsig, H.; Elkj r, C. F.; Helveg, S.; Chorkendorff, I.; Sehested, J., *Science* **2016,** *352*, 969-974.
15. Yang, Y.; Evans, J.; Rodriguez, J. A.; White, M. G.; Liu, P., *Phys. Chem. Chem. Phys.* **2010,** *12*, 9909-9917.
16. Hu, Z. M.; Takahashi, K.; Nakatsuji, H., *Surf. Sci.* **1999,** *442*, 90-106.
17. Nakatsuji, H.; Hu, Z. M., *Int. J. Quantum Chem.* **2000,** *77*, 341-349.
18. Rasmussen, P.; Kazuta, M.; Chorkendorff, I., *Surf. Sci.* **1994,** *318*, 267-280.
19. Grabow, L.; Mavrikakis, M., *ACS Catal.* **2011,** *1*, 365-384.
20. Graciani, J.; Mudiyanselage, K.; Xu, F.; Baber, A. E.; Evans, J.; Senanayake, S. D.; Stacchiola, D. J.; Liu, P.; Hrbek, J.; Sanz, J. F., *Science* **2014,** *345*, 546-550.
21. Tao, X.; Wang, J.; Li, Z.; Ye, Q., *Comput. Theor. Chem.* **2013,** *1023*, 59-64.
22. Studt, F.; Sharafutdinov, I.; Abild-Pedersen, F.; Elkjar, C. F.; Hummelshoj, J. S.; Dahl, S. ; Chorkendorff, I.; Norskov, J. K., *Nature Chem.* **2014,** *6*, 320-324.
23. Martin, O.; Martin, A. J.; Mondelli, C.; Mitchell, S.; Segawa, T. F.; Hauert, R.; Drouilly, C.; Curulla-Ferre, D.; Perez-Ramirez, J., *Angew. Chem. Int. Ed.* **2016,** *55*, 6261-6265.
24. Ye, J.; Liu, C.; Mei, D.; Ge, Q., *ACS Catal.* **2013,** *3*, 1296-1306.
25. Sun, K.; Fan, Z.; Ye, J.; Yan, J.; Ge, Q.; Li, Y.; He, W.; Yang, W.; Liu, C.-J., *J. CO_2 Util.* **2015,** *12*, 1-6.
26. Mei, D.; Zhu, X.; Wu, C.; Ashford, B.; Williams P.T., Tu, X., *Appl. Catal. B: Environ.* **2016,** *182*, 525-532.
27. Mei, D., Zhu, X., He, Y. L., Yan, J. D., Tu, X., *Plasma Sources Sci. Technol.* **2015**, *24*, 015011.
28. Snoeckx, R., Bogaerts, A., *Chem. Soc. Rev.* **2017**, *46*, 5805-5863.
29. Yi, Y.; Zhou, J.; Guo, H.; Zhao, J.; Su, J.; Wang, L.; Wang, X.; Gong, W., *Angew. Chem. Int. Ed.* **2013,** *125*, 8604-8607.
30. Tu, X., Whitehead, J. C., *Int. J. Hydrog. Energy* **2014**, *39*, 9658-9669.
31. Tu, X.; Whitehead, J. C., *Appl. Catal. B: Environ.* **2012,** *125*, 439-448.
32. Fridman, A., *Plasma Chemistry*. Cambridge University Press: 2008; p 259-318.
33. Zou, J. J.; Liu, C. J., *Carbon Dioxide as Chemical Feedstock, Wiley-VCH* **2010**, 267-290.
34. Hayashi, N.; Yamakawa, T.; Baba, S., *Vacuum* **2006,** *80*, 1299-1304.
35. Jwa, E.; Lee, S.; Lee, H.; Mok, Y., *Fuel Process. Technol.* **2013,** *108*, 89-93.
36. Arita, K.; Iizuka, S., *J. Mater. Sci. Chem. Eng.* **2015,** *3*, 69-77.

37. Eliasson, B.; Kogelschatz, U.; Xue, B.; Zhou, L. M., *Ind. Eng. Chem. Res.* **1998,** *37*, 3350-3357.
38. Kano, M.; Satoh, G.; Iizuka, S., *Plasma Chem. Plasma Process.* **2012,** *32*, 177-185.
39. Amouroux, J.; Cavadias, S.; Doubla, A., Carbon dioxide reduction by non-equilibrium electrocatalysis plasma reactor. In *IOP Conference Series: Materials Science and Engineering*, 2011; Vol. 19, p 012005.
40. Nizio, M.; Albarazi, A.; Cavadias, S.; Amouroux, J.; Galvez, M. E.; Da Costa, P., *Int. J. Hydro. Energy* **2016,** *41*, 11584-11592.
41. Zeng, Y.; Tu, X., *IEEE Trans. Plasma Sci.* **2016,** *44*, 405-411.
42. Zeng, Y.; Tu, X., *J. Phys. D: Appl. Phys.* **2017,** *50*, 184004.
43. Bill, A.; Eliasson, B.; Kogelschatz, U.; Zhou, L. M., *Stud. in Surf. Sci. Catal.* **1998,** *114*, 541-544.
44. Wang, Z. j.; Zhao, Y.; Cui, L.; Du, H.; Yao, P.; Liu, C. j., *Green Chem.* **2007,** *9*, 554-559.
45. Martinez Guerrero, R.; Hernandez-Gordillo, A.; Santes, V.; Vargas Garcia, J. R.; Escobar, J.; Diaz-Garcia, L.; Diaz Barriga Arceo, L.; Garibay Febles, V., *J. Chem.* **2014,** *2014,* 679281, DoI: 10.1155/2014/679281.
46. de la Pena O'Shea, V.; Alvarez-Galvan, M.; Fierro, J.; Arias, P., *Appl. Catal. B: Environ.* **2005,** *57*, 191-199.
47. Aerts, R.; Somers, W.; Bogaerts, A., *ChemSusChem* **2015**, *8*, 702-716.
48. Tsang, W.; Hampson, R., *J. Phys. Chem. Ref. Data* **1986,** *15*, 1087-1279.
49. Polanyi, J. C., *Science* **1987,** *236*, 680-690.
50. Gordon, E.; Ivanov, B.; Perminov, A.; Balalaev, V., *Chem. Phys.* **1978,** *35*, 79-89.
51. Baulch, D.; Cobos, C.; Cox, R.; Esser, C.; Frank, P.; Just, T.; Kerr, J.; Pilling, M.; Troe, J.; Walker, R., *J. Phys. Chem. Ref. Data* **1992,** *21*, 411-734.
52. Curran, H., *Int. J. Chem. Kinetics* **2006,** *38*, 250-275.
53. Brudnik, K.; Gola, A. A.; Jodkowski, J. T., *J. Molecular Modeling* **2009,** *15*, 1061-1066.
54. Cherian, M.; Rhodes, P.; Simpson, R.; Dixon-Lewis, G., *Symposium (International) on Combustion* **1981,** *18*, 385-396.
55. Tsuboi, T.; Katoh, M.; Kikuchi, S.; Hashimoto, K., *Jap. J. Appl. Phys.* **1981,** *20*, 985-992.
56. Tu, X.; Gallon, H. J., Whitehead, J. C., *J. Phys: D: Appl. Phys.* **2011**, *44*, 482003.
57. Whitehead, J. C., *J. Phy. D: Appl. Phys.* **2016,** *49*, 243001.
58. Yang, X.; Kattel, S.; Senanayake, S. D.; Boscoboinik, J. A.; Nie, X.; Graciani, J. s.; Rodriguez, J. A.; Liu, P.; Stacchiola, D. o. J.; Chen, J. G., *J. Am. Chem. Soc.* **2015,** *137*, 10104-10107.
59. Kattel, S., Yan, B., Chen, J. G., Liu, P., *J. Catal.* **2016**, 343, 115-126.
60. Stere, C.; Anderson, J. A.; Chansai, S.; Delgado, J. J.; Goguet, A.; Graham, W. G.; Hardacre, C.; Taylor, R.; Tu, X.; Wang, Z.; Yang, H., *Angew. Chem. Int. Ed.* **2017**, *56*, 5579-5583.
61. Stere, C. E.; Adress, W.; Burch, R.; Chansai, S.; Goguet, A.; Graham, W. G.; Hardacre, C., *ACS Catal.* **2015**, *5*, 956-964.
62. Wang, L.; Yi, Y.; Guo, Y.; Zhao, Y.; Zhang, J.; Guo, H., *Plasma Process. Polymers* **2016,** *14*, e1600111.
63. Nozaki, T.; Muto, N.; Kadio, S.; Okazaki, K., *Catal. Today* **2004,** *89*, 67-74.
64. Jaeger, R.; Homann, K.; Kuhlenbeck, H.; Freund, H.-J., *Chem. Phys. Lett.* **1993,** *203*, 41-45.
65. Ferri, D.; Burgi, T.; Baiker, A., *Phys. Chem. Chem. Phys.* **2002,** *4*, 2667-2672.